

Rift zone architecture and inflation-driven seismicity of Mauna Loa volcano

John D. Wilding¹ and Zachary E. Ross¹

¹Seismological Laboratory, California Institute of Technology

Key Points:

- We construct a new catalog of 91,770 relocated earthquakes at Mauna Loa volcano spanning 2011-2023
- The new catalog details a decade of nonstationary inflation-related seismicity and detailed structure in the caldera and rift zones
- Our observations can provide a framework for understanding future episodes of pre-eruptive seismic unrest at Mauna Loa

Corresponding author: J.D. Wilding, jwilding@caltech.edu

Abstract

The 2022 eruption at Mauna Loa, Hawai‘i, marked the first extrusive activity from the volcano after 38 years of quiescence. The eruption was preceded by several years of seismic unrest in the vicinity of the volcano’s summit. Characterizing the structure and dynamics of seismogenic features within Mauna Loa during this pre-eruptive interval may provide insights into how pre- and co-eruptive processes manifest seismically at the volcano. In particular, the extent to which seismicity may be used to forecast the location and timing of future eruptions is unclear. To address these questions, we construct a catalog of relocated seismicity on Mauna Loa spanning 2011-2023. Our earthquake locations image complex, sub-kilometer-scale seismogenic structures in the caldera and southwest rift zone. We additionally identify a set of streaks of seismicity in the volcano’s northwest flank that are radially oriented about the summit. Using a rate-and-state friction model for earthquake occurrences, we demonstrate that the seismicity rate in this region can be modeled as a function of the stressing history caused by magma accumulation beneath the summit. Finally, we observe a mid-2019 step change in the seismicity rate in the Ka’oiki region that may have altered the stress state of the northeast rift zone in the three years before the eruption. Our observations provide a framework for interpreting future seismic unrest at Mauna Loa.

1 Introduction

Monitoring of seismic unrest at active volcanoes can help to identify periods of elevated eruptive risk, in particular through detection of subsurface magma accumulation. Pre-eruptive patterns of seismicity, however, can differ between volcanoes and across individual eruptions, such that near-term forecasting often benefits from detailed knowledge of a volcano’s internal structure and dynamics (Pesicek et al., 2021, 2018). In 2022, Mauna Loa volcano (Figure 1) erupted for the first time since 1984, following years of elevated seismicity and deformation in the near-summit region (Thelen et al., 2017; Maher et al., 2023). In the context of global volcanology, pre-eruptive patterns of behavior at Mauna Loa are comparatively well understood, which has allowed for some degree of advance warning for its most recent three eruptions (1975, 1984, 2022) (Decker et al., 1995; Maher et al., 2023). However, our understanding of how seismic unrest at Mauna Loa relates to summit inflation and magma dynamics continues to lag behind comparable efforts at its neighboring volcano, Kilauea (Figure 1).

This gap in understanding can be attributed (at least in part) to Mauna Loa’s quiescence in recent decades (P. G. Okubo, 1995). Mauna Loa was eruptively quiescent between its 1984 and 2022 eruptions, although there was evidence of magma accumulation beneath the summit of Mauna Loa during this period (Burgess & Roman, 2021; Poland et al., 2012). During the same period of time, Kilauea was erupting nearly continuously; this eruptive activity, combined with the development of techniques that can process large amounts of digital data from the Hawaiian Volcano Observatory (HVO) seismic network, has led to rapid progress in our understanding of Kilauea’s caldera and rift zone structure (Shelly & Thelen, 2019; Matoza et al., 2021), subcaldera magma storage (Matoza et al., 2014; Crozier & Karlstrom, 2021), pre-eruptive stress changes (Liu et al., 2022), and dike intrusion processes (Lengliné et al., 2021). Largely due to its eruptive quiescence in the digital recording era, analogous structures and processes at Mauna Loa have proven difficult to characterize.

One important set of open questions pertains to the role and significance of pre-eruptive seismicity around the volcano. While earthquake rates generally increase prior to eruptions (Lengliné et al., 2008; Decker et al., 1995), the span of time between the onset of seismicity and the eventual eruption is variable; the 1984 eruption, for instance, was preceded by approximately 6 years of accelerating seismicity rates, whereas the 1975 eruption was preceded by only 1 year of seismic unrest (P. G. Okubo, 1995). Acceler-

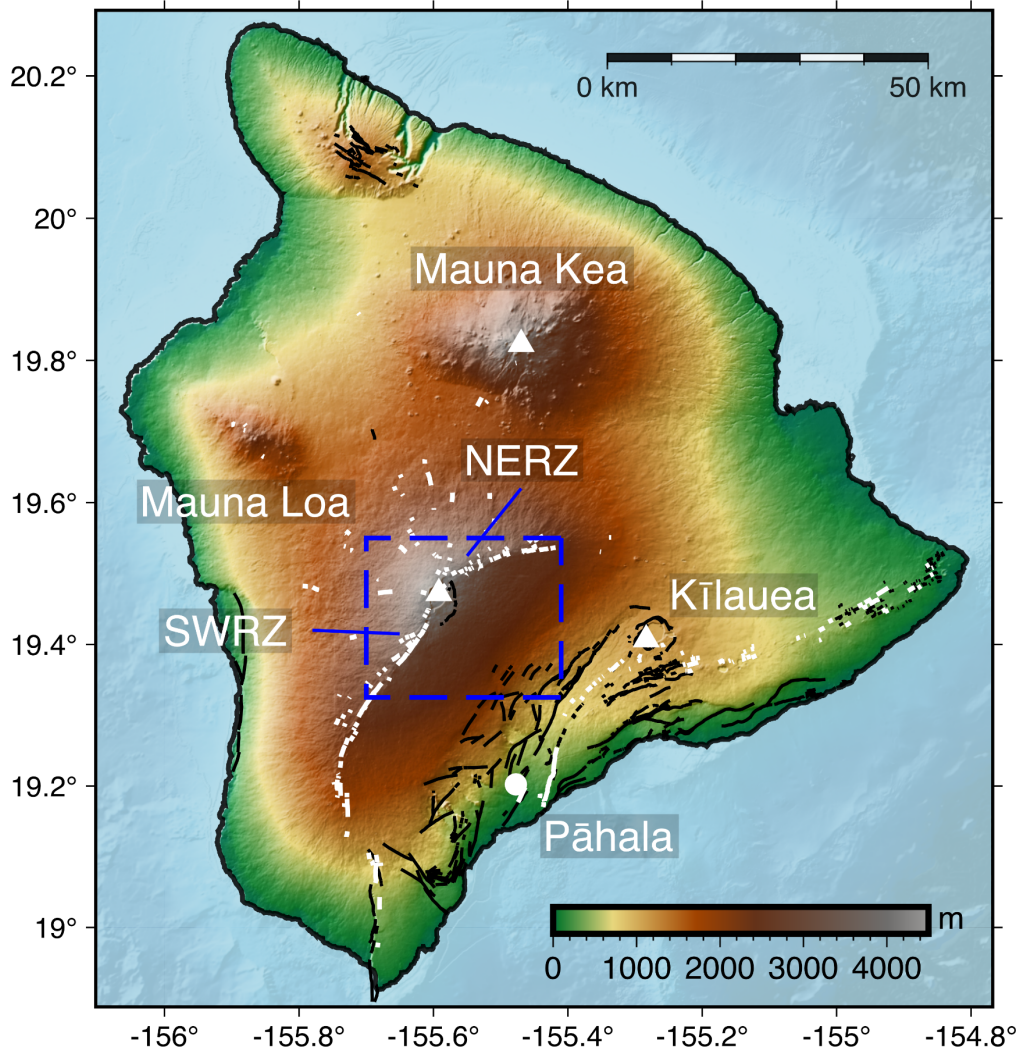


Figure 1. Map view of the island of Hawai'i. White lines are mapped fissure locations and black lines are mapped fault traces (Wolfe (compiler) & Morris, 1996; Sherrod et al., 2021). Mauna Loa, Kīlauea, and Mauna Kea volcanoes are denoted by white triangles. NERZ and SWRZ denote Mauna Loa's northeast rift zone and southwest rift zone, respectively. Our study region is denoted by the dashed blue box (Figure 2).

ating rates of seismicity from 0-6 km bsl along Mauna Loa’s northwest flank (NWF) have been suggested to reflect increased inflationary stresses and portend eruptions (Lockwood et al., 1987). NWF seismicity has been interpreted as delineating a failed rift zone (Baher et al., 2003), but the seismic structure of the region is yet to be imaged and analyzed in detail. Additionally, the influence of eruptions at Kilauea on eruptive potential at Mauna Loa is ambiguous; while some studies have identified anticorrelated patterns of activity between the two volcanoes (Klein, 1982; Przeor et al., 2022), others have identified correlated short-term variations of magma supply to Kilauea and Mauna Loa (Poland et al., 2012; Burgess & Roman, 2021), potentially related to shared components of the volcanoes’ magma supply systems (Wright & Klein, 2006; Wilding et al., 2023).

The internal structure of Mauna Loa’s rift zones is also not well characterized. Structural heterogeneity in ocean island volcano rift zones may exert a first-order control on the downrift propagation of magma (Patrick et al., 2020; Varugu & Amelung, 2021; Woods et al., 2019); thus, a detailed understanding of rift zone structure may be important for forecasting the eventual location and timing of eruptions. Additionally, eruptions at Mauna Loa may begin within the caldera or along either of the southwest (SWRZ) or northeast (NERZ) rift zones, but the factors controlling the initial site of an eruption are not well understood. This question is significant, as lava flows that erupt from the SWRZ are capable of reaching populated coastal areas in as little as 3.5 hours (Gregg et al., 2004). Inflation of the summit magma system and large earthquakes along the décollement beneath the volcano’s eastern flank at 7-10 km bsl may clamp or unclamp segments of the rift zones, influencing the relative favorability of intrusions at different sites, but it remains to be shown if detectable stress changes influenced the location of the 2022 NERZ eruption (Walter & Amelung, 2006; Amelung et al., 2007).

In November 2022, Mauna Loa erupted from both the NERZ and caldera following several years of inflation (Maher et al., 2023; Thelen et al., 2017). This eruption was recorded by 11 near-summit seismic stations on the Mauna Loa edifice and represents an opportunity to investigate the questions outlined previously. The eruption was also the first from Mauna Loa in 38 years; the possibility of renewed eruptive activity highlights the importance of improving our understanding of Mauna Loa’s seismic activity.

In this study, our contributions are as follows. To characterize patterns of pre- and co-eruptive behavior at Mauna Loa, we build a new seismicity catalog for Mauna Loa with deep learning algorithms for the period January 2011 to March 2023 (Figure 2). Using this catalog, we image high-resolution structures within and surrounding the Mauna Loa summit and detail the seismic behavior of the volcano in the decade prior to its 2022 eruption. We identify complex sub-kilometer-scale structure in the SWRZ. We show that the rates of earthquakes in the NWF can be predicted from the stressing rate history from magmatic inflation beneath the summit. Furthermore, we observe a mid-2019 increase in slip along the Ka’oiki décollement that may have altered the stress state of the summit region and promoted the 2022 NERZ intrusion and eruption.

2 Methods

2.1 Seismicity catalog construction

To construct our catalog, we download continuous data for the period January 2011 – March 2023 from 11 seismic stations on Mauna Loa operated by the Hawaiian Volcano Observatory (HVO) (Figure S1). We build a dataset of 3.6 million P and 3.3 million S arrivals from these data using the automated phase picking algorithm PhaseNet (Zhu & Beroza, 2019). We then associate these picks into 571,048 events using the GaMMA algorithm (Zhu et al., 2022), requiring a minimum of 8 picks per event, and calculate approximate magnitudes using the rapid response magnitude algorithm of Picozzi et al. (2018).

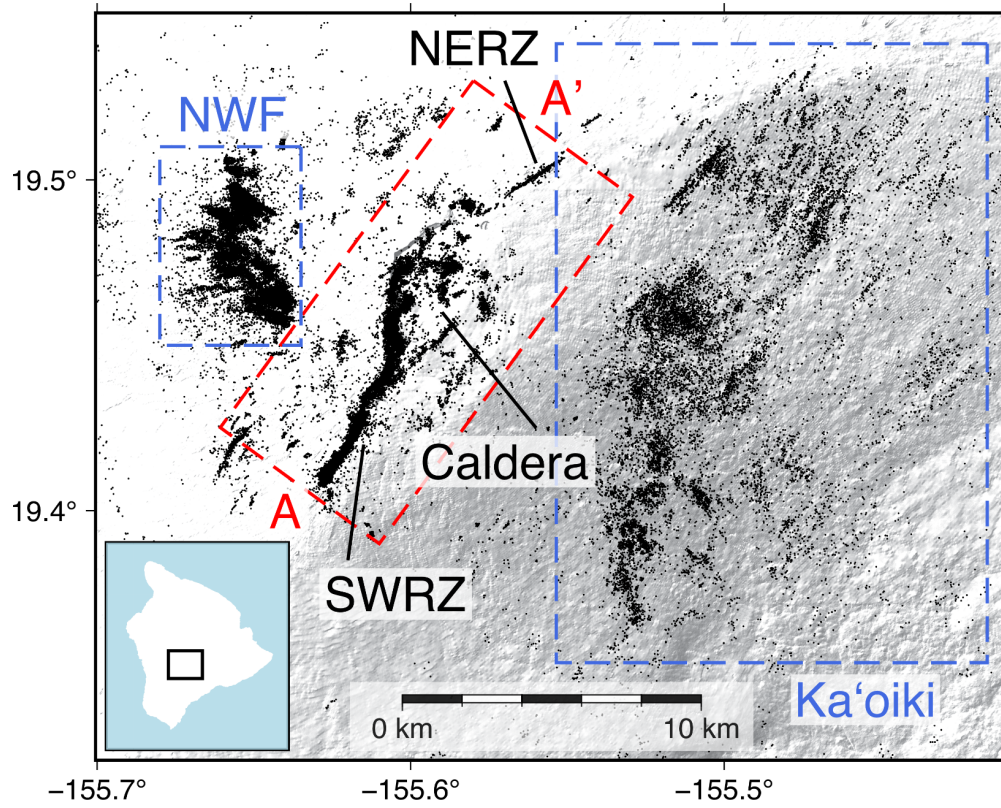


Figure 2. Overview of the Mauna Loa summit region with relocated seismicity from our catalog. The northwest flank region (NWF) and Ka'oiki region are boxed in blue. The caldera, northeast rift zone (NERZ), and southwest rift zone (SWRZ) are within the A-A' profile, plotted in greater detail in Figure 3a.

We determine earthquake locations using the HypoSVI algorithm, a variational inference technique for determining hypocenter posterior distributions (Smith et al., 2022). This method was previously applied successfully to a catalog for Hawai'i for the period 2019-2022 (Wilding et al., 2023). First, we determine a set of initial locations using a 1D velocity model extracted from the 3D tomographic model of Lin et al. (2014). Because our focus is on Mauna Loa, we discard events outside of $[-155.75^\circ\text{W}, -155.35^\circ\text{W}]$ and $[19.28^\circ\text{N}, 19.62^\circ\text{N}]$. We also discard events with depths greater than 3 km above sea level, as well as events deeper than 20 km below sea level, for which the network aperture is insufficient to constrain accurate depths. Then, we use an iterative process to improve the locations progressively. We calculate the median absolute deviation (MAD) of all remaining travel-time residuals ($\text{MAD} = 0.13 \text{ s}$) and discard outlier picks with absolute travel-time residuals greater than $3 \cdot \text{MAD}$. We then discard events with fewer than 8 picks after this filtering step. Our use of a small subset of the HVO seismic network introduces the possibility of mislocating seismicity from out-of-network regions, especially Kilauea and Mauna Kea (Figure 1), which were both quite seismically active during our study period (Wech et al., 2020; Wilding et al., 2023). To identify mislocated events, we associate events in our catalog with their counterparts in the HVO and Wilding et al. (2023) catalogs. We identify 3,866 events which have been mislocated and discard these events. Finally, we search our catalog for pairs of events occurring within 10 s of one another, which may represent single events which have erroneously been split into multiple detections by the GaMMA algorithm; we find and discard 1,194 such events.

Following these steps, we iteratively update our locations using source-specific station terms (SSSTs) to correct for unmodeled 3D velocity structure (Richards-Dinger & Shearer, 2000). We use k -nearest neighbor clustering to calculate SSSTs for each event using the median of travel-time residuals of the nearest k earthquakes. We test multiple values of k between 500 and 10,000 and observe that earthquake locations improve with increasing k up to $k = 5000$, and show minimal improvement for $k > 5000$ (Figure S2); for our final locations, we set $k = 5000$. Travel-time residuals cease to decrease appreciably after 10 iterations of the SSST procedure (Figure S3), at which point we halt the procedure and extract locations for the 131,890 events remaining in our catalog. We then perform waveform-based relative relocation using GrowClust (Trugman & Shearer, 2017) and successfully relocate 91,770 events (Figure 2).

2.2 GNSS data processing and deformation extraction

Transient stress changes induced by deformation of the near-summit magma system can influence rates of seismicity at Mauna Loa and other volcanoes (Varugu & Amelung, 2021; Wauthier et al., 2019). To complement our analysis of the seismicity catalog, we retrieve GNSS data to characterize deformation sources occurring during our study period. We download GPS data from 26 Mauna Loa-adjacent stations from the Nevada Geodetic Laboratory spanning 2011-2022 (Blewitt et al., 2018). We correct for long-term plate motion by fitting a linear function to the position timeseries of the Mauna Kea station MKEA and subtracting the linear function from the Mauna Loa position data, following the processing methodology of Varugu and Amelung (2021). Using the software package DISSTANS, we estimate and remove the high-frequency common mode error using independent component analysis (Köhne et al., 2023). We then fit the GPS timeseries at all stations with periodic (annual and biannual) and transient components (parameterized by degree-2 spline functions). Splines and periodic functions are fit to each station's timeseries using L1-regularized least squares to promote sparsity. The fits to the GPS data are further regularized with a spatial L0 penalty that promotes similar, sparse spline coefficients for neighboring GPS stations (Köhne et al., 2023). Finally, we remove the periodic signal components from each station and retain the transient components for analysis.

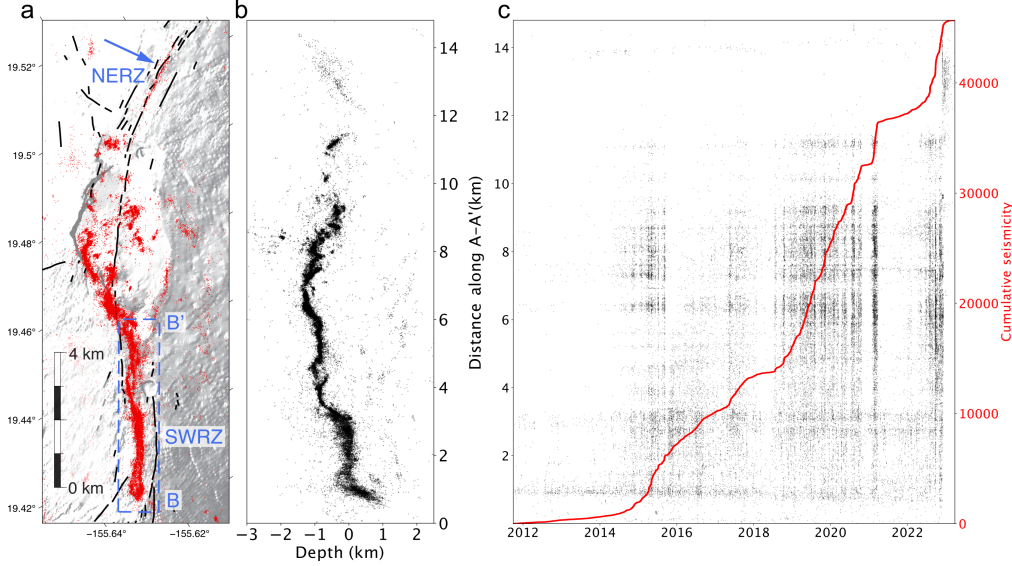


Figure 3. (a) Detailed view of profile A-A' from Fig. 2. The NERZ and SWRZ extending from the Mauna Loa caldera are labeled; the boxed region around the SWRZ (profile B-B') is plotted in greater detail in Fig. 3. Black lines are mapped fissure traces (Wolfe (compiler) & Morris, 1996; Sherrod et al., 2021); seismicity is plotted in red for visibility. The B-B' box enclosed by the dashed blue line is plotted in greater detail in Fig. 3. The blue arrow denotes the thin lineament of NERZ seismicity accompanying the 2022 eruption. (b) Depth view of seismicity along the A-A' profile. (c) Seismicity along the A-A' profile through time. The red line represents cumulative seismicity from the beginning of our catalog.

3 Results

3.1 Mauna Loa caldera and rift zone structure

Our catalog reveals extensive seismicity hosted on discrete structures throughout the caldera and SWRZ (Figure 3). Within the caldera, most seismicity occurs along the southwest bounding fault, with additional earthquakes occurring in the center of the caldera and along the southeast boundary. We also identify seismicity to the east of the caldera that may reflect deformation along an outer ring fault structure. Seismicity in the SWRZ is confined to a limited vertical extent (~ 2 km), similar to earthquakes observed at Kilauea's rift zones (Gillard et al., 1996). We identify complicated seismogenic structures in the SWRZ at kilometer to sub-kilometer scales (Figure 4). The southernmost 1.5 km of the rift zone (between 0.5 and 2 km along the B-B' profile) is bifurcated into two laterally subparallel strands of seismicity. We also observe a curved, hook-like structure between 3 and 4 km along the A-A' profile that is similar in morphology to normal fault structures mapped in mature rift zones (Childs et al., 1995). Smaller curvilinear structures may also be present between 4-6 km along the A-A' profile, suggesting a high degree of structural maturity.

The temporal history of seismicity in the caldera and SWRZ over the 2011-2023 period (Figure 3c) is characterized by alternating periods of activity and relative quiescence. During these active periods, seismicity occurs throughout the entire caldera and SWRZ; we find no evidence for seismicity migration up- or down-rift during these episodes. Notably, we identify a region to the immediate southeast of the caldera (Figure S4) that is almost completely quiescent in our catalog until approximately 2 months prior to the

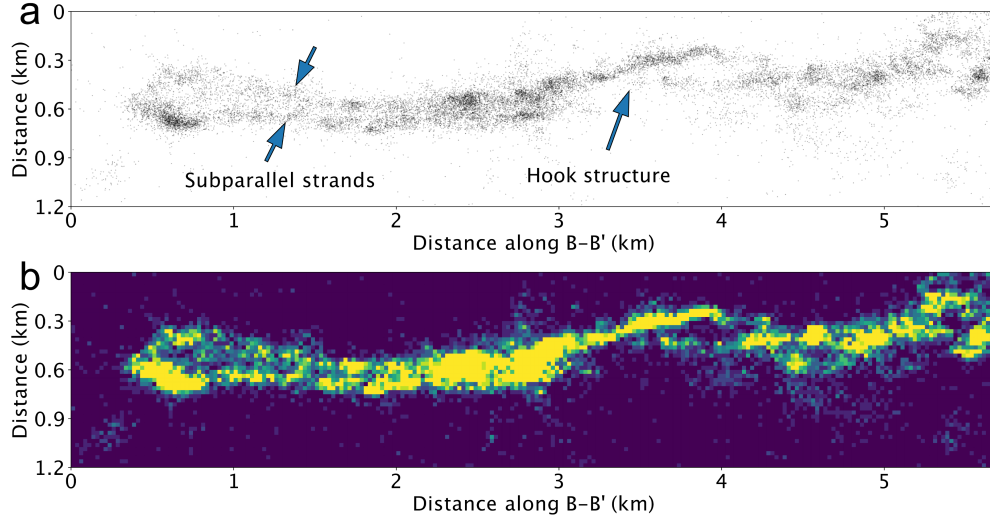


Figure 4. (a) Detailed view of seismicity in the SWRZ. Individual features referred to in the text are labeled for clarity. Subparallel strands are visible between 0.5 and 2 km along the B-B' profile. The seismicity also defines curvilinear, hook-like structures between 3 and 6 km along the B-B' profile. (b) Density plot of seismicity to emphasize the labeled structures.

2022 eruption, at which point it produces hundreds of earthquakes. This temporal pattern suggests that previously quiescent components of the ring fault system activated shortly before the eruption. The NERZ is quiescent in our catalog until the eruption, at which point a burst of seismicity occurs along an elongated, linear feature aligned with the trend of the NERZ fissures (denoted by a red arrow in Figure 3a). Following the activity associated with the November 2022 eruption, the caldera and rift zones revert to seismic quiescence.

Beneath the summit and rift zones, the vast majority of seismicity locates above 1 km bsl and there is a lack of coherent structure to the seismicity at greater depths (Figure S5). These observations are consistent with other seismicity catalogs of Mauna Loa (Matoza et al., 2021; USGS Hawaiian Volcano Observatory (HVO), 1956). The lack of seismicity at mid-to-lower crustal depths beneath the Mauna Loa magmatic system stands in marked contrast to Kilauea, where sub-caldera long-period earthquakes extending to 15 km depth are consistently identified in seismic catalogs (Matoza et al., 2021; Wilding et al., 2023).

3.2 Deformational structures

East of the summit, seismicity in the Ka'oiki seismic zone occurs primarily along a nearly flat basal décollement at depths of 8-10 km (Figure 5) (Wyss et al., 1992). Approaching the north, faulting becomes listric, as suggested by Walter and Amelung (2006). Our catalog delineates NE-striking faults that were also resolved in the catalog of Matoza et al. (2021). Previous focal mechanism studies in this region suggest that the NE-striking faults are right-lateral strike-slip faults that, along with the décollement, accommodate deformation from volcanic loading and flank instability (Walter & Amelung, 2004; Bryan & Johnson, 1991; Wyss et al., 1992). In July 2019, we observe a step increase in the Ka'oiki seismicity rate that is unlikely to be related to instrumental effects. The seismic network configuration on Mauna Loa is largely stabilized by August 2013. The seismicity rate

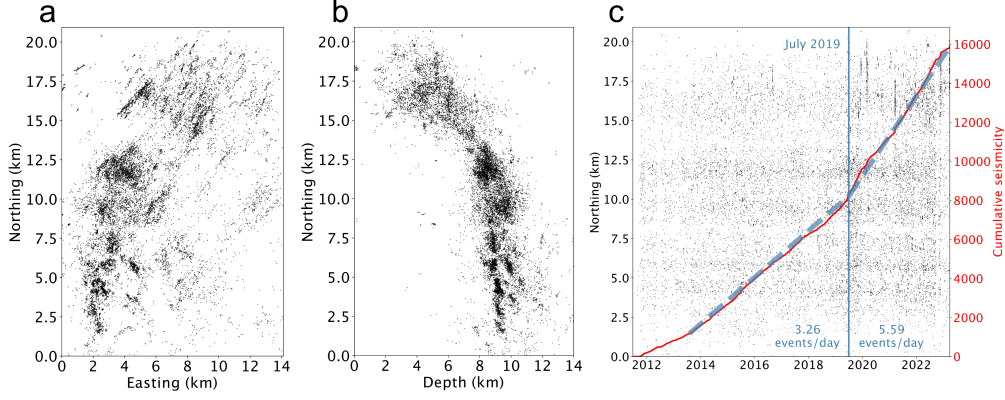


Figure 5. (a) Map view of seismicity in the Ka'oiki region boxed in Figure 2. (b) Depth view of seismicity in the Ka'oiki region. (c) Seismicity in the Ka'oiki region through time. The red line represents cumulative seismicity from the beginning of our catalog. The vertical blue line is 1 July 2019. The dashed lines are plotted to emphasize the increase in seismicity rate beginning in roughly July 2019.

in Ka'oiki is roughly linear between August 2013 and July 2019 at a rate of 3.26 events/day; after July 2019, the seismicity rate suddenly increases to 5.59 events/day (Figure 5c).

Seismicity in the NWF occurs along a collection of discrete lineaments, or streaks, that are oriented roughly radially with respect to the Mauna Loa summit (Figure 6a). The streaks are confined to a 4 km by 6 km semi-planar surface dipping to the north-northeast at approximately 32° . The depth of seismicity within these streaks (2-6 km) is shallower than the depth of the décollement beneath Mauna Loa's west flank (8-10 km) (Wyss et al., 1992), indicating that these earthquakes are likely not hosted on the décollement. In contrast to Ka'oiki, the seismicity rate in the NWF is highly nonstationary, with individual streaks hosting discrete bursts of activity that persist for weeks to months (Figure 6c). Additionally, the temporal patterns of seismicity in the northern half of the NWF differ significantly from the temporal patterns in the southern half; to illustrate this difference, we subdivide NWF seismicity into "northern" and "southern" regions separated at 19.48°N and examine their seismicity rates separately (Figure 7b). The NWF is essentially quiescent before June 2014, generating 86 earthquakes/year on average. The rate of NWF earthquakes increases to 1,261 earthquakes/year between June 2014 and October 2018; during this period, seismicity is mostly confined to the south. In October 2018, the seismicity rate in the northern NWF rapidly increases, and seismic productivity remains high until the 2022 eruption. Between October 2018 and December 2022, the NWF produces an average of 4,865 earthquakes/year; following the eruption, the NWF reverts to quiescence.

During our study period, the subcaldera magmatic system at Mauna Loa evinced nonstationary rates of magma accumulation and changes in magma chamber geometry (Varugu & Amelung, 2021). In particular, Varugu and Amelung (2021) inverted GPS and InSAR data from 2014-2020 for deformation source models, identifying evolving magma chamber geometries and potencies. To identify potential relationships between summit inflation and NWF seismicity, we compare GPS data to the seismicity rate history in the NWF. We observe that changes in the NWF seismicity rate correspond in time with transient deformation episodes recorded on the NWF-adjacent GPS stations ALEP, TOUO, and PHAN. For each of these stations, we calculate the direction of maximum horizontal deformation between 2011 and 2022 from the transient components of motion extracted

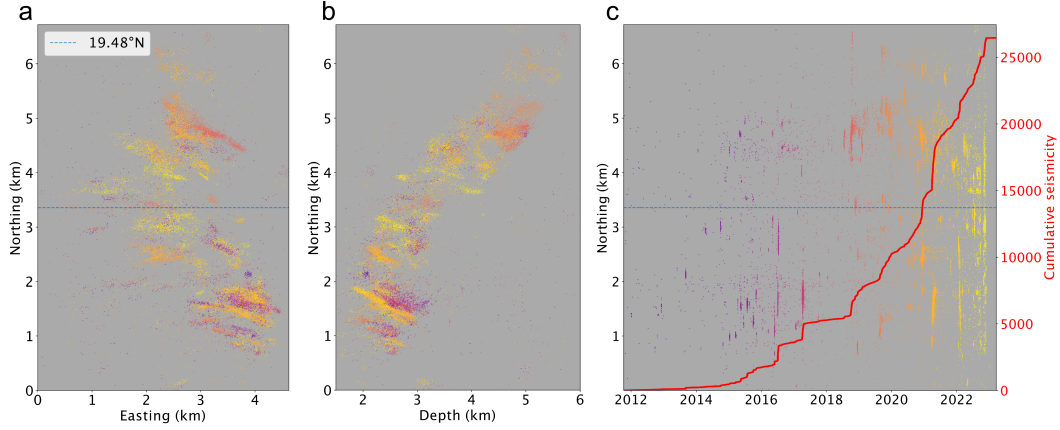


Figure 6. (a) Map view of the seismicity of the NWF region (boxed in Fig. 1). Seismicity is colored by time to emphasize the burst-like activity within each streak. The dashed blue line is the line of latitude at 19.48°N that separates southern and northern NWF seismicity. (b) Depth view of seismicity of the NWF region, colored by time. (c) Seismicity in the NWF region through time. The color scale is the same used in (a) and (b). The red line represents cumulative seismicity in the NWF. The dashed blue line corresponds to 19.48°N.

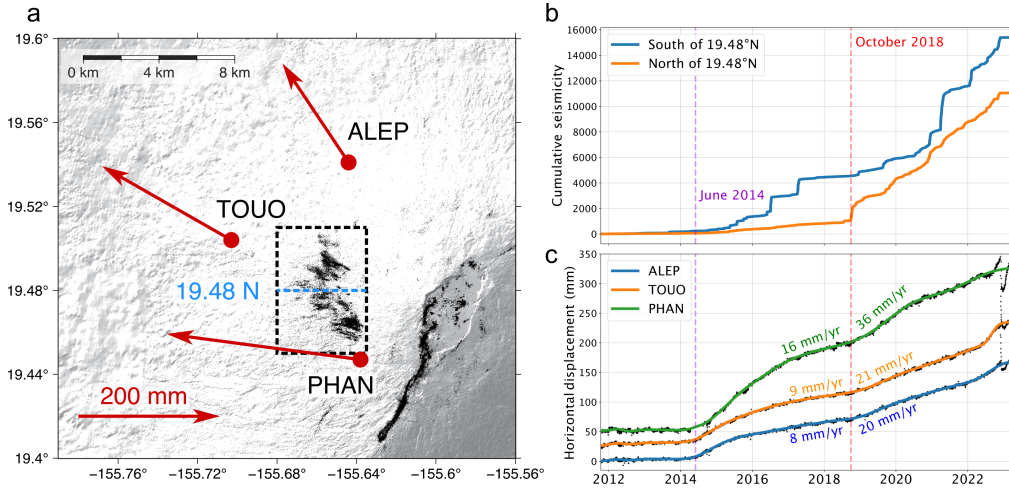


Figure 7. (a) Direction and magnitude of maximum horizontal displacement over the 2011–2022 period for NWF-adjacent GPS stations ALEP, TOUO, and PHAN. The NWF region is boxed with a dashed line; the dashed blue line is 19.48°N. (b) Cumulative seismicity south (blue) and north (orange) of 19.48°N in the NWF region. The seismicity rate in the NWF undergoes distinct increases beginning in June 2014 and October 2018. (c) Timeseries of horizontal displacement in the direction of maximum displacement for GPS stations ALEP, TOUO, and PHAN. Black dots represent residuals for each station calculated by the DISSTANS fitting algorithm. The seismicity rate increases illustrated in (b) correspond to increases in horizontal velocity for all three stations.

by DISSTANS. The maximum horizontal deformation directions and the position time-series projected along the maximum deformation direction are plotted for these three stations in Figure 7ac. While deformation is minimal before 2014, a deformation transient beginning in June 2014 coincides with the onset of a gradual increase in NWF seismicity. Between 2014 and 2017, most seismicity in the NWF is restricted to the southern NWF. After 2017, we observe a slowing in the rate of deformation and a return to seismic quiescence, although GPS velocities remain elevated relative to 2012-2014. In October 2018, we observe a sudden increase in horizontal velocity at all three GPS stations. This increase is coincident with renewed seismic activity in the NWF, including a sudden increase in seismicity in the northern NWF. After October 2018, deformation and seismicity in the NWF continue until the 2022 eruption. The deformation transients we observe here are broadly consistent with those reported by Varugu and Amelung (2021), who identify three distinct phases of summit deformation spanning 2014-2015, 2015-2018, and 2018-2020, respectively. These correspondences indicate a possible relationship between summit deformation and NWF seismicity.

To assess whether summit deformation is capable of driving the NWF seismicity through static stress transfer (King et al., 1994), we perform Coulomb stress (ΔCS) modeling. We determine a receiver plane in the NWF by fitting a plane to the seismicity (Figure 8a). We calculate Coulomb stress on the receiver plane induced by the time-varying dike inflation and Mogi source solutions obtained by Varugu and Amelung (2021) for the Mauna Loa summit. For simplicity, we assume a westward rake along the entire receiver plane, consistent with previous focal mechanisms determined for the region (Bryan & Johnson, 1991; Gillard et al., 1992). Varugu and Amelung (2021) invert for three stationary models spanning the periods January 2014 to August 2015, August 2015 to April 2018, and April 2018 to May 2020, respectively; to calculate Coulomb stress after the end of their study period, we extend the geometry and seismic potency of their 2018-2020 sources to December 2022. We calculate stress using the formulation of Okada (1992) for half-space deformation. Following Varugu and Amelung (2021), we assume a Poisson's ratio of 0.25 and a shear modulus of 16 GPa. We assume a value of 0.35 for the effective shear modulus μ' ; we test several values of μ' between 0.2 and 0.4 and found that our results are not qualitatively sensitive to μ' within this range (Figure S6).

The results of the Coulomb stress calculations are plotted in Figure 8b-d. The Coulomb stress is slightly negative on the receiver plane during 2014-2015, with a median stressing rate of -0.008 MPa/yr, consistent with seismic quiescence in the NWF. During 2015-2018, the Coulomb stressing rate shifts to positive across the receiver plane with a median value of 0.027 MPa/yr, coincident with an increase in NWF seismicity. The region of maximum stressing rate in this period (~ 0.17 MPa/yr) is proximal to the concentrated seismicity south of 19.48° . The rate of Coulomb stress remains positive over 2018-2022, during which time we also observe a northward shift in the region of maximum stressing and a sustained increase in NWF seismicity north of 19.48° . Although these source models lack fine spatiotemporal resolution, the qualitative correspondences between Coulomb stress and patterns of seismicity suggest that the rate of NWF seismicity is strongly tied to stress changes from inflation of Mauna Loa's shallow magma system.

To investigate whether the rate of seismicity in the NWF can be modeled as a function of Coulomb stress time history, we employ the model of J. Dieterich (1994), which relates stress history to cumulative seismicity in a rate-and-state friction framework. The model can be written as (Heimisson & Segall, 2018)

$$\frac{N}{r} = t_a \log\left(\frac{1}{t_a} \int_0^t K(t') dt' + 1\right) \quad (1)$$

where t_a is a characteristic aftershock decay time, N is the cumulative number of earthquakes through time t , and r is the background rate of seismicity. K is an integral kernel which, under the assumption that changes in normal stress are small relative to the

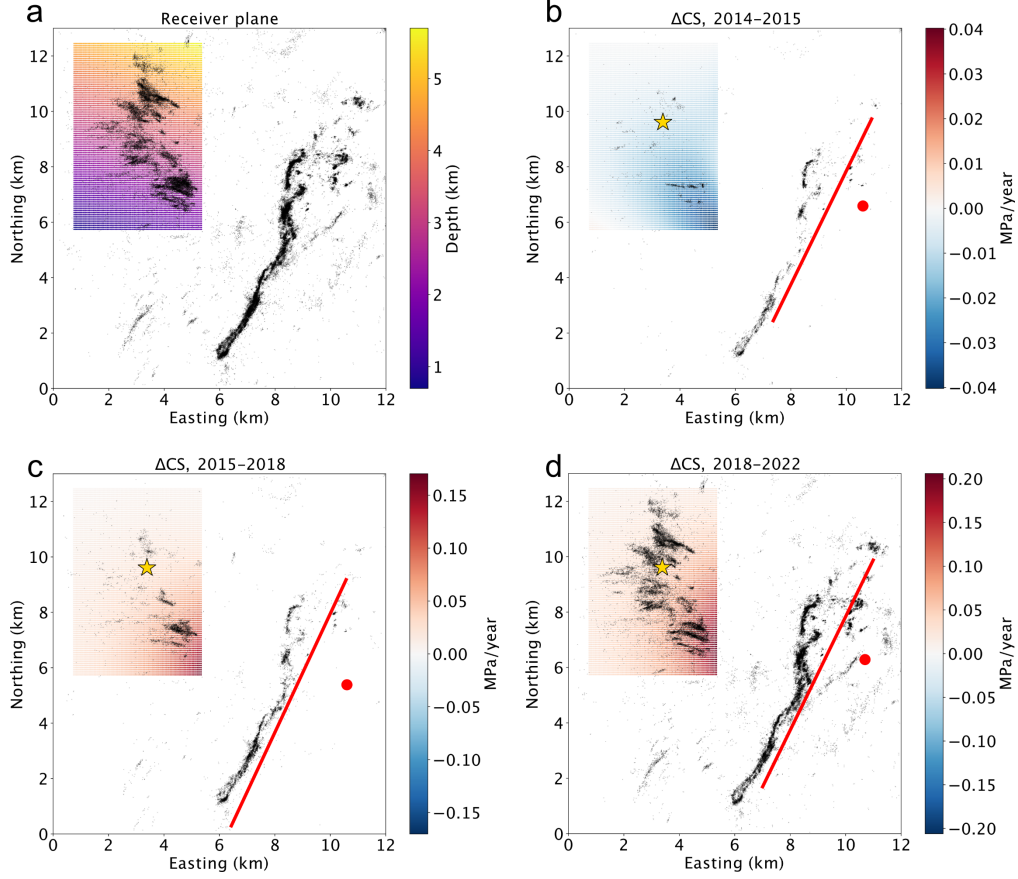


Figure 8. (a) Depth of the receiver plane fitted to NWF seismicity. (b-d) Coulomb stressing rates on the NWF receiver plane assuming a westward rake and the geometries and potencies of Varugu and Amelung (2021). In each plot, seismicity occurring during the time range of the model is plotted. The red dots and lines represent the locations of an imposed Mogi source and opening plane during each discrete time period. The gold star is the median location of all seismicity in the NWF; the Coulomb stress timeseries plotted in Figure 9 is measured at this point.

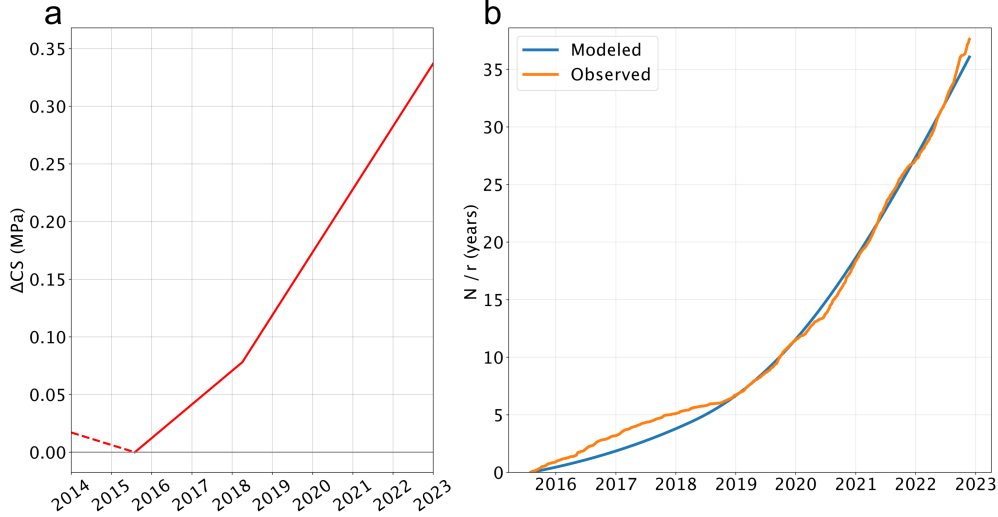


Figure 9. (a) Coulomb stress history for the point marked by a gold star in Figure 8. The dashed segment from January 2014 to August 2015, during which the Coulomb stressing rates is negative, is not included in the input to the seismicity rate modeling. (b) Observed (orange) and modeled (blue) seismicity history in the NWF.

background normal stress, can be formulated in terms of Coulomb stress change (Heimisson & Segall, 2018; Siorattanakul et al., 2022):

$$K(t) = \exp(\Delta CS(t) \cdot \frac{S_{inf}}{A\sigma}) \quad (2)$$

where ΔCS is the Coulomb stress change history normalized from 0 at $t = 0$ to 1 at the end of the stress time series t_{inf} , A is a fault constitutive parameter, σ is normal stress, and S_{inf} is the Coulomb stress at the end of the stress timeseries. We define ΔCS as the Coulomb stress history at the centroid of NWF seismicity spanning August 2015, when the stressing rate becomes positive, to December 2022.

To define N , we subset NWF seismicity, identify a magnitude of completeness of 0.25 (Figure S7), and remove events below magnitude 0.25. The magnitude-filtered catalog of NWF seismicity includes several discrete swarms of activity that take place on the order of days to weeks, far below the temporal resolution of the deformation source models of Varugu and Amelung (2021). In order to avoid potential biases to the fitting procedure caused by these short-term clusters, we perform nearest-neighbor-based declustering of the catalog using the method of Zaliapin and Ben-Zion (2013) (Figure S8), using an estimated b-value of 1.22 (Figure S7). We then calculate N using the declustered catalog. We define r as the average seismicity rate of the declustered catalog between August 2013 (at which point the seismic network geometry is mostly stable) and August 2015 (78.6 events/yr).

Our model assumes that σ is constant throughout the NWF, although, because of the dip of the receiver plane, the true value of σ likely varies with depth. Under these simplifying assumptions, the model relating stress history to N only consists of two parameters, $A\sigma$ and t_a . We perform a grid search to identify best-fitting values and achieve a good fit with $A\sigma = 63.6$ kPa and $t_a = 12.4$ yr (Figure 9). The quality of the fit, despite the simplifying assumptions involved, suggests that NWF seismicity can be related to stressing caused by summit deformation using a simple rate-and-state triggering model.

4 Discussion

4.1 Rift zone structure

The precise earthquake locations that we obtain in our catalog allow us to image the internal structures of Mauna Loa’s SWRZ. Seismic structure in the SWRZ is characterized by geometric complexity, with a curvilinear, hook-like structure and subparallel strands of seismicity distributed over an area roughly 500 m in the rift-perpendicular direction (Figure 4). These features are consistent with continuing lateral growth of the rift zone as it evolves (J. H. Dieterich, 1988). Similar hook structures are routinely identified in developing normal fault systems (Gudmundsson et al., 1993; Childs et al., 1995), including within volcanic rift zones in Iceland (Acocella et al., 2000), where they are interpreted to arise from the interaction of developing extensional fractures. In these systems, growing normal faults evolve from an “underlapping” stage, where the faults are separated in the rift-parallel direction, to an “overlapping” state, where the faults overlap in the rift-perpendicular direction (Acocella et al., 2000). The hook structure we image overlaps significantly with another strand of seismicity, suggesting that a mature fault system has developed to accommodate lateral growth of the SWRZ.

Segmented, parallel tracks of seismicity, similar to those we observe in the SWRZ, have been documented along the path of a dike intrusion in Bardarbunga, where they were interpreted as parallel magma paths during dike propagation (Woods et al., 2019). Woods et al. (2019) suggested that the parallel segmentation may have reflected a complicated spatiotemporal pattern of dike propagation, where magma initially moved through one path and stalled for approximately one day before breaching the other, parallel path, where it ultimately erupted from the surface. If the parallel strands in the SWRZ are interpreted as two possible magma pathways, downrift dike propagation in the SWRZ may likewise be complicated by structural factors. Structural barriers to dike propagation have previously been suggested in the SWRZ (Varugu & Amelung, 2021). Our results highlight the possibility that structural complexity in the SWRZ may influence downrift magma propagation and the location and timing of rift eruptions; understanding the behavior of magma within the rift zone may thus be important to inform short-term hazard forecast models.

4.2 NWF seismicity

Our stress modeling indicates that the seismicity rates of the streaks within Mauna Loa’s NWF are highly sensitive to stressing caused by summit deformation. Similarly, seismicity rates have been shown to be sensitive to transient stress perturbations on Kilauea’s south flank (J. Dieterich et al., 2000; Segall et al., 2006) and upper east rift zone (Wauthier et al., 2019). This sensitivity raises the possibility that patterns of seismicity in the NWF can be used as an indicator of unrest in the Mauna Loa magma system, as has been suggested previously (Lockwood et al., 1987). Seismic monitoring of this feature may also be able to provide insight into changes in the state of stress in the Mauna Loa edifice, potentially improving the spatiotemporal resolution of deformation models.

Seismicity within Kilauea’s upper east rift zone is thought to concentrate into lineaments along a stress concentration where a vertically-dipping strike-slip fault within the rift contacts an underlying high-temperature cumulate body (Gillard et al., 1996); in this model, seismicity occurs along the stress concentration at the narrow contact between the brittle overlying rock and the relatively weaker cumulates. Similar streaks of seismicity are observed along the brittle-ductile transition in California (Rubin et al., 1999); in spatially distributed fault systems, such streaks have also been observed to occur in parallel (Shearer, 2002). We propose that the seismicity lineaments within the NWF are manifestations of a similar deformation process along a planar contact between an overlying brittle layer and an underlying cumulate-bearing layer. In the absence of a well-defined rift zone in the NWF, active lineaments are laterally distributed along this pla-

nar contact rather than concentrating along a single lineament. Previous gravity studies have not resolved the existence of high-density, cumulate-like material beneath Mauna Loa's NWF (Denlinger & Flinders, 2022; Kauahikaua et al., 2000), suggesting that cumulate material in the NWF may be tightly distributed preferentially along the seismicity lineaments. These structures could conceivably serve to supply magma to the distributed network of radially oriented eruptive fissures on the surface of the NWF (Figure 1) (Riker et al., 2009). The lack of a proper rift zone along the NWF has been interpreted to result from buttressing of the NWF by Hualalai and Mauna Kea (Baher et al., 2003); this buttressing might be responsible for our proposed laterally distributed deformation.

Our proposed model for the NWF seismicity may also be relevant for the Nāmakani Seismic Zone on the northwest flank of Kilauea. Early earthquake locations in Nāmakani were interpreted as forming a normal fault dipping southeast (P. Okubo & Nakata, 2003). More recent catalogs, however, have identified streaks of seismicity distributed across a plane that dips away from the Kilauea summit (Matoza et al., 2021; Wilding et al., 2023), in a similar orientation to the NWF. Increased seismicity has also been reported in Nāmakani in the weeks prior to rift zone and summit intrusions (P. Okubo & Nakata, 2003). Kilauea's northwest flank is buttressed by Mauna Loa's edifice and NERZ in a similar manner to Mauna Loa's NWF, and is underlain by high-density (Denlinger & Flinders, 2022) and electrically resistive (Hoversten et al., 2022) material. These properties hint that the Nāmakani Seismic Zone could represent another instance of laterally distributed deformation at a planar contact with a ductile cumulate layer that may be sensitive to inflation of the sub-caldera magmatic system.

4.3 Rift zone eruptive favorability

Our catalog documents a decade of seismicity and deformation within the Mauna Loa edifice prior to its 2022 eruption. We suggest that the deformation we observe might have contributed to a stress state that promoted the eventual intrusion into the NERZ. Following eight years of steady activity along the basal décollement and strike-slip faults of the Ka'oiki region, we identify a significant increase in the seismicity rate after July 2019 (Figure 5c). Coulomb stress modeling indicates that both slumping of the Mauna Loa pile along the Ka'oiki décollement and right-lateral motion along the northern strike-slip faults can reduce normal stresses in the upper NERZ (Walter & Amelung, 2006). Accelerated slip along Ka'oiki's décollement and northern strike-slip faults might have contributed to increased unclamping of the intruded segment of the NERZ in the three years before Mauna Loa's 2022 eruption, promoting conditions for an eventual NERZ intrusion and eruption.

The increase in seismicity rate in Ka'oiki, which started just a few months after the 2018 Kilauea caldera collapse sequence, may reflect accelerated slip precipitated by stress transfer from Kilauea. A previous catalog identified a large swarm of long-period seismicity 30 km beneath the summit of Kilauea in July 2019; concurrently, a mantle swarm 25 km southwest of Kilauea at 40 km depth beneath the village of Pāhala (Figure 1) experienced an order-of-magnitude increase in seismicity rate (Wilding et al., 2023). These mantle earthquakes have been interpreted as reflecting an episode of renewed magma supply to Kilauea volcano following its 2018 caldera collapse (Wilding et al., 2023). The correspondence between increased seismicity in the mantle and at Ka'oiki suggests that deformational structures that can influence the magma system of Mauna Loa may in turn be influenced by stress transfer from Kilauea's magma system.

In the decade prior to Mauna Loa's 2022 NERZ eruption, our catalog documents significant, ongoing seismicity in the SWRZ and near-total quiescence in the NERZ. This pattern indicates that comparing the relative rates of earthquakes along each rift zone may not serve as a reliable indicator of the initial location of future eruptions. The re-

sults of our rate-and-state friction modeling, however, do suggest that seismicity may be able to provide insights into the evolving state of stress within the Mauna Loa edifice. Future efforts to improve the spatiotemporal resolution of deformation source models may provide greater insight into controls on eruption location at Mauna Loa.

5 Conclusions

We develop a comprehensive catalog of relocated seismicity for the Mauna Loa edifice spanning 2011-2023 to study near-summit structures and pre- and co-eruptive patterns of earthquake behavior. Our catalog details geometrical complexity in the SWRZ and a decade of nonstationary seismicity in the NWF region that can be attributed to stressing caused by inflation of the sub-caldera magma system. We also observe an acceleration of seismicity in the Ka'oiki seismic zone approximately three years prior to Mauna Loa's 2022 NERZ eruption. The deformation evidenced by our seismic catalog suggests that the NERZ may have been progressively unclamped in the years before the eruption, creating favorable stress conditions for an eventual intrusion into the NERZ. Our results shine new light on the evolving stress state in the volcanic edifice and may be used to aid in future monitoring efforts at Mauna Loa. They also serve to improve our physical understanding of near-summit structures in the Mauna Loa edifice and how they influence, and are influenced by, changing magma storage conditions. The historical record indicates that eruptions at Mauna Loa are clustered in time (Klein, 1982); our results provide additional context to aid in the interpretation of possible future unrest at Mauna Loa.

Acknowledgments

JDW and ZER received support from NSF award EAR-2239666. The facilities of EarthScope Consortium were used for access to waveforms, related metadata, and/or derived products used in this study. These services are funded through the Seismological Facility for the Advancement of Geoscience (SAGE) Award of the National Science Foundation under Cooperative Agreement EAR-1724509. The authors would like to thank Tobias Köhne for productive discussions regarding the use of the software package DISSTANS. ZER is grateful to the David and Lucile Packard Foundation for supporting this study through a Packard Fellowship.

6 Open Research

All seismic data used in this study from the Hawaiian Volcano Observatory network are publicly available for download from the EarthScope consortium (USGS Hawaiian Volcano Observatory (HVO), 1956). GNSS data are available for download from the Nevada Geodetic Laboratory (Blewitt et al., 2018).

References

- Acocella, V., Gudmundsson, A., & Funicello, R. (2000, September). Interaction and linkage of extension fractures and normal faults: examples from the rift zone of Iceland. *Journal of Structural Geology*, 22(9), 1233–1246. Retrieved 2024-01-23, from <https://www.sciencedirect.com/science/article/pii/S0191814100000316> doi: 10.1016/S0191-8141(00)00031-6
- Amelung, F., Yun, S.-H., Walter, T. R., Segall, P., & Kim, S.-W. (2007, May). Stress Control of Deep Rift Intrusion at Mauna Loa Volcano, Hawaii. *Science*, 316(5827), 1026–1030. Retrieved 2024-01-23, from <https://www.science.org/doi/10.1126/science.1140035> (Publisher: American Association for the Advancement of Science) doi: 10.1126/science.1140035
- Baher, S., Thurber, C., Roberts, K., & Rowe, C. (2003, December). Relocation

- of seismicity preceding the 1984 eruption of Mauna Loa Volcano, Hawaii: Delineation of a possible failed rift. *Journal of Volcanology and Geothermal Research*, 128(4), 327–339. Retrieved 2022-12-26, from <https://www.sciencedirect.com/science/article/pii/S0377027303001999> doi: 10.1016/S0377-0273(03)00199-9
- Blewitt, G., Hammond, W., & Kreemer, C. (2018, September). Harnessing the GPS Data Explosion for Interdisciplinary Science. *Eos*, 99. Retrieved 2024-02-21, from <https://eos.org/project-updates/harnessing-the-gps-data-explosion-for-interdisciplinary-science> doi: 10.1029/2018EO104623
- Bryan, C. J., & Johnson, C. E. (1991, April). Block tectonics of the island of Hawaii from a focal mechanism analysis of basal slip. *Bulletin of the Seismological Society of America*, 81(2), 491–507. Retrieved 2022-12-26, from <https://doi.org/10.1785/BSSA0810020491> doi: 10.1785/BSSA0810020491
- Burgess, M. K., & Roman, D. C. (2021). Ongoing (2015-) Magma Surge in the Upper Mantle Beneath the Island of Hawaii. *Geophysical Research Letters*, 48(7), e2020GL091096. Retrieved 2021-09-01, from <https://agupubs.onlinelibrary.wiley.com/doi/abs/10.1029/2020GL091096> doi: 10.1029/2020GL091096
- Childs, C., Watterson, J., & Walsh, J. J. (1995, June). Fault overlap zones within developing normal fault systems. *Journal of the Geological Society*, 152(3), 535–549. Retrieved 2024-01-23, from <https://doi.org/10.1144/gsjgs.152.3.0535> doi: 10.1144/gsjgs.152.3.0535
- Crozier, J., & Karlstrom, L. (2021). Wavelet-Based Characterization of Very-Long-Period Seismicity Reveals Temporal Evolution of Shallow Magma System Over the 2008–2018 Eruption of Kilauea Volcano. *Journal of Geophysical Research: Solid Earth*, 126(6), e2020JB020837. Retrieved 2024-01-23, from <https://onlinelibrary.wiley.com/doi/abs/10.1029/2020JB020837> doi: 10.1029/2020JB020837
- Decker, R. W., Klein, F. W., Okamura, A. T., & Okubo, P. G. (1995). Forecasting Eruptions of Mauna Loa Volcano, Hawaii. In *Mauna Loa Revealed: Structure, Composition, History, and Hazards* (pp. 337–348). American Geophysical Union (AGU). Retrieved 2024-01-23, from <https://onlinelibrary.wiley.com/doi/abs/10.1029/GM092p0337> doi: 10.1029/GM092p0337
- Denlinger, R. P., & Flinders, A. (2022, March). Density structure of the island of Hawai'i and the implications for gravity-driven motion of the south flank of Kilauea Volcano. *Geophysical Journal International*, 228(3), 1793–1807. Retrieved 2022-03-29, from <https://doi.org/10.1093/gji/ggab398> doi: 10.1093/gji/ggab398
- Dieterich, J. (1994). A constitutive law for rate of earthquake production and its application to earthquake clustering. *Journal of Geophysical Research: Solid Earth*, 99(B2), 2601–2618. Retrieved 2021-09-20, from <https://onlinelibrary.wiley.com/doi/abs/10.1029/93JB02581> doi: 10.1029/93JB02581
- Dieterich, J., Cayol, V., & Okubo, P. (2000, November). The use of earthquake rate changes as a stress meter at Kilauea volcano. *Nature*, 408(6811), 457–460. Retrieved 2024-01-23, from <https://www.nature.com/articles/35044054> (Number: 6811 Publisher: Nature Publishing Group) doi: 10.1038/35044054
- Dieterich, J. H. (1988). Growth and persistence of Hawaiian volcanic rift zones. *Journal of Geophysical Research: Solid Earth*, 93(B5), 4258–4270. Retrieved 2021-09-05, from <https://agupubs.onlinelibrary.wiley.com/doi/abs/10.1029/JB093iB05p04258> doi: 10.1029/JB093iB05p04258
- Gillard, D., Rubin, A. M., & Okubo, P. (1996, November). Highly concentrated seismicity caused by deformation of Kilauea's deep magma system. *Nature*, 384(6607), 343–346. Retrieved 2021-09-01, from <https://www.nature.com/articles/384343a0> (Bandiera_abtest: a Cg_type: Nature Research Journals

- Number: 6607 Primary.atype: Research Publisher: Nature Publishing Group)
doi: 10.1038/384343a0
- Gillard, D., Wyss, M., & Nakata, J. S. (1992). A seismotectonic model for western Hawaii based on stress tensor inversion from fault plane solutions. *Journal of Geophysical Research: Solid Earth*, 97(B5), 6629–6641. Retrieved 2024-01-23, from <https://onlinelibrary.wiley.com/doi/abs/10.1029/91JB02709> doi: 10.1029/91JB02709
- Gregg, C. E., Houghton, B. F., Paton, D., Swanson, D. A., & Johnston, D. M. (2004, August). Community preparedness for lava flows from Mauna Loa and Hualālai volcanoes, Kona, Hawai'i. *Bulletin of Volcanology*, 66(6), 531–540. Retrieved 2024-01-24, from <https://doi.org/10.1007/s00445-004-0338-x> doi: 10.1007/s00445-004-0338-x
- Gudmundsson, A., Brynjolfsson, S., & Jonsson, M. T. (1993, April). Structural analysis of a transform fault-rift zone junction in North Iceland. *Tectonophysics*, 220(1), 205–221. Retrieved 2024-01-23, from <https://www.sciencedirect.com/science/article/pii/0040195193902329> doi: 10.1016/0040-1951(93)90232-9
- Heimisson, E. R., & Segall, P. (2018). Constitutive Law for Earthquake Production Based on Rate-and-State Friction: Dieterich 1994 Revisited. *Journal of Geophysical Research: Solid Earth*, 123(5), 4141–4156. Retrieved 2024-01-23, from <https://onlinelibrary.wiley.com/doi/abs/10.1029/2018JB015656> doi: 10.1029/2018JB015656
- Hoversten, G. M., Gasperikova, E., Mackie, R., Myer, D., Kauahikaua, J., Newman, G. A., & Cuevas, N. (2022). Magnetotelluric Investigations of the Kīlauea Volcano, Hawaii. *Journal of Geophysical Research: Solid Earth*, 127(8), e2022JB024418. Retrieved 2024-02-11, from <https://onlinelibrary.wiley.com/doi/abs/10.1029/2022JB024418> doi: 10.1029/2022JB024418
- Kauahikaua, J., Hildenbrand, T., & Webring, M. (2000, October). Deep magmatic structures of Hawaiian volcanoes, imaged by three-dimensional gravity models. *Geology*, 28(10), 883–886. Retrieved 2022-12-26, from [https://doi.org/10.1130/0091-7613\(2000\)28<883:DMSOHV>2.0.CO;2](https://doi.org/10.1130/0091-7613(2000)28<883:DMSOHV>2.0.CO;2) doi: 10.1130/0091-7613(2000)28<883:DMSOHV>2.0.CO;2
- King, G. C. P., Stein, R. S., & Lin, J. (1994, June). Static stress changes and the triggering of earthquakes. *Bulletin of the Seismological Society of America*, 84(3), 935–953. Retrieved 2024-01-23, from <https://doi.org/10.1785/BSSA0840030935> doi: 10.1785/BSSA0840030935
- Klein, F. W. (1982, March). Patterns of historical eruptions at Hawaiian volcanoes. *Journal of Volcanology and Geothermal Research*, 12(1), 1–35. Retrieved 2022-07-11, from <https://www.sciencedirect.com/science/article/pii/0377027382900026> doi: 10.1016/0377-0273(82)90002-6
- Köhne, T., Riel, B., & Simons, M. (2023, January). Decomposition and Inference of Sources through Spatiotemporal Analysis of Network Signals: The DIS-STANS Python package. *Computers & Geosciences*, 170, 105247. Retrieved 2024-01-23, from <https://www.sciencedirect.com/science/article/pii/S0098300422001960> doi: 10.1016/j.cageo.2022.105247
- Lengliné, O., Duputel, Z., & Okubo, P. G. (2021, January). Tracking dike propagation leading to the 2018 Kīlauea eruption. *Earth and Planetary Science Letters*, 553, 116653. Retrieved 2024-01-23, from <https://www.sciencedirect.com/science/article/pii/S0012821X20305975> doi: 10.1016/j.epsl.2020.116653
- Lengliné, O., Marsan, D., Got, J.-L., Pinel, V., Ferrazzini, V., & Okubo, P. G. (2008). Seismicity and deformation induced by magma accumulation at three basaltic volcanoes. *Journal of Geophysical Research: Solid Earth*, 113(B12). Retrieved 2022-11-28, from <https://onlinelibrary.wiley.com/doi/abs/10.1029/2008JB005937> doi: 10.1029/2008JB005937

- Lin, G., Shearer, P. M., Matoza, R. S., Okubo, P. G., & Amelung, F. (2014). Three-dimensional seismic velocity structure of Mauna Loa and Kilauea volcanoes in Hawaii from local seismic tomography. *Journal of Geophysical Research: Solid Earth*, 119(5), 4377–4392. Retrieved 2022-12-02, from <https://onlinelibrary.wiley.com/doi/abs/10.1002/2013JB010820> doi: 10.1002/2013JB010820
- Liu, Z., Liang, C., Huang, H., Wang, C., & Cao, F. (2022). Seismic Velocity Variations at Different Depths Reveal the Dynamic Evolution Associated With the 2018 Kilauea Eruption. *Geophysical Research Letters*, 49(3), e2021GL093691. Retrieved 2024-01-23, from <https://onlinelibrary.wiley.com/doi/abs/10.1029/2021GL093691> doi: 10.1029/2021GL093691
- Lockwood, J. P., Dvorak, J. J., English, T. T., Koyanagi, R. Y., Okamura, Arnold T., Summers, Marjorie L., & Tanigawa, Wilfred R. (1987). Mauna Loa 1974–1984: A decade of intrusive and extrusive activity. In R. Decker, T. Wright, & P. Stauffer (Eds.), *Volcanism in Hawaii* (Vol. 2, pp. 1019–1185).
- Maher, S. P., Dawson, P., Hotovec-Ellis, A., Thelen, W. A., Jolly, A., Bennington, N., ... Dotray, P. (2023, August). Characterizing and Locating Seismic Tremor during the 2022 Eruption of Mauna Loa Volcano, Hawai'i, with Network Covariance. *The Seismic Record*, 3(3), 228–238. Retrieved 2024-01-23, from <https://doi.org/10.1785/0320230020> doi: 10.1785/0320230020
- Matoza, R. S., Okubo, P. G., & Shearer, P. M. (2021). Comprehensive High-Precision Relocation of Seismicity on the Island of Hawai'i 1986–2018. *Earth and Space Science*, 8(1), e2020EA001253. Retrieved 2021-08-17, from <https://agupubs.onlinelibrary.wiley.com/doi/abs/10.1029/2020EA001253> doi: 10.1029/2020EA001253
- Matoza, R. S., Shearer, P. M., & Okubo, P. G. (2014). High-precision relocation of long-period events beneath the summit region of Kilauea Volcano, Hawai'i, from 1986 to 2009. *Geophysical Research Letters*, 41(10), 3413–3421. Retrieved 2022-10-15, from <https://onlinelibrary.wiley.com/doi/abs/10.1002/2014GL059819> doi: 10.1002/2014GL059819
- Okada, Y. (1992, April). Internal deformation due to shear and tensile faults in a half-space. *Bulletin of the Seismological Society of America*, 82(2), 1018–1040. Retrieved 2024-01-23, from <https://doi.org/10.1785/BSSA0820021018> doi: 10.1785/BSSA0820021018
- Okubo, P., & Nakata, J. S. (2003). Tectonic pulses during Kilauea's current long-term eruption. In *The Pu'u 'Ō'ō-Kūpaianaha eruption of Kilauea Volcano, Hawai'i: The first 20 years* (pp. 173–186).
- Okubo, P. G. (1995). A Seismological Framework for Mauna Loa Volcano, Hawaii. In *Mauna Loa Revealed: Structure, Composition, History, and Hazards* (pp. 187–197). American Geophysical Union (AGU). Retrieved 2024-01-23, from <https://onlinelibrary.wiley.com/doi/abs/10.1029/GM092p0187> doi: 10.1029/GM092p0187
- Patrick, M. R., Houghton, B. F., Anderson, K. R., Poland, M. P., Montgomery-Brown, E., Johanson, I., ... Elias, T. (2020, November). The cascading origin of the 2018 Kilauea eruption and implications for future forecasting. *Nature Communications*, 11(1), 5646. Retrieved 2023-06-30, from <https://www.nature.com/articles/s41467-020-19190-1> (Number: 1 Publisher: Nature Publishing Group) doi: 10.1038/s41467-020-19190-1
- Pesicek, J. D., Ogburn, S. E., & Prejean, S. G. (2021). Indicators of Volcanic Eruptions Revealed by Global M4+ Earthquakes. *Journal of Geophysical Research: Solid Earth*, 126(3), e2020JB021294. Retrieved 2024-02-22, from <https://onlinelibrary.wiley.com/doi/abs/10.1029/2020JB021294> doi: 10.1029/2020JB021294
- Pesicek, J. D., Wellik, J. J., Prejean, S. G., & Ogburn, S. E. (2018). Prevalence of Seismic Rate Anomalies Preceding Volcanic Eruptions in Alaska. *Frontiers*

- in *Earth Science*, 6. Retrieved 2024-02-22, from <https://www.frontiersin.org/articles/10.3389/feart.2018.00100>
- Picozzi, M., Bindi, D., Spallarossa, D., Di Giacomo, D., & Zollo, A. (2018, June). A rapid response magnitude scale for timely assessment of the high frequency seismic radiation. *Scientific Reports*, 8(1), 8562. Retrieved 2024-01-23, from <https://www.nature.com/articles/s41598-018-26938-9> (Number: 1 Publisher: Nature Publishing Group) doi: 10.1038/s41598-018-26938-9
- Poland, M. P., Miklius, A., Jeff Sutton, A., & Thornber, C. R. (2012, April). A mantle-driven surge in magma supply to Kilauea Volcano during 2003–2007. *Nature Geoscience*, 5(4), 295–300. Retrieved 2022-06-02, from <http://www.nature.com/articles/ngeo1426> doi: 10.1038/ngeo1426
- Przeor, M., D’Auria, L., Pepe, S., Tizzani, P., & Cabrera-Pérez, I. (2022, November). Elastic interaction between Mauna Loa and Kilauea evidenced by independent component analysis. *Scientific Reports*, 12(1), 19863. Retrieved 2022-12-26, from <https://www.nature.com/articles/s41598-022-24308-0> (Number: 1 Publisher: Nature Publishing Group) doi: 10.1038/s41598-022-24308-0
- Richards-Dinger, K. B., & Shearer, P. M. (2000, May). Earthquake locations in southern California obtained using source-specific station terms. *Journal of Geophysical Research: Solid Earth*, 105(B5), 10939–10960. Retrieved 2022-04-12, from <http://doi.wiley.com/10.1029/2000JB900014> doi: 10.1029/2000JB900014
- Riker, J. M., Cashman, K. V., Kauahikaua, J. P., & Montierth, C. M. (2009, June). The length of channelized lava flows: Insight from the 1859 eruption of Mauna Loa Volcano, Hawai‘i. *Journal of Volcanology and Geothermal Research*, 183(3), 139–156. Retrieved 2024-01-24, from <https://www.sciencedirect.com/science/article/pii/S0377027309001395> doi: 10.1016/j.jvolgeores.2009.03.002
- Rubin, A. M., Gillard, D., & Got, J.-L. (1999, August). Streaks of microearthquakes along creeping faults. *Nature*, 400(6745), 635–641. Retrieved 2024-01-23, from <https://www.nature.com/articles/23196> (Number: 6745 Publisher: Nature Publishing Group) doi: 10.1038/23196
- Segall, P., Desmarais, E. K., Shelly, D., Miklius, A., & Cervelli, P. (2006, July). Earthquakes triggered by silent slip events on Kilauea volcano, Hawaii. *Nature*, 442(7098), 71–74. Retrieved 2021-09-01, from <https://www.nature.com/articles/nature04938> (Bandiera_abtest: a Cg_type: Nature Research Journals Number: 7098 Primary_atype: Research Publisher: Nature Publishing Group) doi: 10.1038/nature04938
- Shearer, P. M. (2002). Parallel fault strands at 9-km depth resolved on the Imperial Fault, Southern California. *Geophysical Research Letters*, 29(14), 19–19–4. Retrieved 2024-01-23, from <https://onlinelibrary.wiley.com/doi/abs/10.1029/2002GL015302> doi: 10.1029/2002GL015302
- Shelly, D. R., & Thelen, W. A. (2019). Anatomy of a Caldera Collapse: Kilauea 2018 Summit Seismicity Sequence in High Resolution. *Geophysical Research Letters*, 46(24), 14395–14403. Retrieved 2021-08-31, from <https://agupubs.onlinelibrary.wiley.com/doi/abs/10.1029/2019GL085636> doi: 10.1029/2019GL085636
- Sherrod, D. R., Sinton, J. M., Watkins, S. E., & Brunt, K. M. (2021). *Geologic map of the State of Hawaii* (USGS Numbered Series No. 3143). Reston, VA: U.S. Geological Survey. Retrieved 2022-11-03, from <http://pubs.er.usgs.gov/publication/sim3143> doi: 10.3133/sim3143
- Sirorattanakul, K., Ross, Z. E., Khoshmanesh, M., Cochran, E. S., Acosta, M., & Avouac, J.-P. (2022). The 2020 Westmorland, California Earthquake Swarm as Aftershocks of a Slow Slip Event Sustained by Fluid Flow. *Journal of Geophysical Research: Solid Earth*, 127(11), e2022JB024693. Retrieved 2024-01-23,

- from <https://onlinelibrary.wiley.com/doi/abs/10.1029/2022JB024693>
doi: 10.1029/2022JB024693
- Smith, J. D., Ross, Z. E., Azizzadenesheli, K., & Muir, J. B. (2022, January). HypoSVI: Hypocentre inversion with Stein variational inference and physics informed neural networks. *Geophysical Journal International*, 228(1), 698–710. Retrieved 2023-06-29, from <https://doi.org/10.1093/gji/ggab309> doi: 10.1093/gji/ggab309
- Thelen, W., Miklius, A., & Neal, C. (2017, October). *Volcanic Unrest at Mauna Loa, Earth's Largest Active Volcano*. Retrieved 2023-06-29, from <http://eos.org/features/volcanic-unrest-at-mauna-loa-earths-largest-active-volcano>
- Trugman, D. T., & Shearer, P. M. (2017, February). GrowClust: A Hierarchical Clustering Algorithm for Relative Earthquake Relocation, with Application to the Spanish Springs and Sheldon, Nevada, Earthquake Sequences. *Seismological Research Letters*, 88(2A), 379–391. Retrieved 2024-01-23, from <https://doi.org/10.1785/0220160188> doi: 10.1785/0220160188
- USGS Hawaiian Volcano Observatory (HVO). (1956). *Hawaiian volcano observatory network* [Dataset]. International Federation of Digital Seismograph Networks. doi: 10.7194/SN/HV
- Varugu, B., & Amelung, F. (2021, May). Southward growth of Mauna Loa's dike-like magma body driven by topographic stress. *Scientific Reports*, 11(1), 9816. Retrieved 2021-09-02, from <https://www.nature.com/articles/s41598-021-89203-6> doi: 10.1038/s41598-021-89203-6
- Walter, T. R., & Amelung, F. (2004). Influence of volcanic activity at Mauna Loa, Hawaii, on earthquake occurrence in the Kaoiki Seismic Zone. *Geophysical Research Letters*, 31(7). Retrieved 2022-12-26, from <https://onlinelibrary.wiley.com/doi/abs/10.1029/2003GL019131> doi: 10.1029/2003GL019131
- Walter, T. R., & Amelung, F. (2006). Volcano-earthquake interaction at Mauna Loa volcano, Hawaii. *Journal of Geophysical Research: Solid Earth*, 111(B5). Retrieved 2022-12-26, from <https://onlinelibrary.wiley.com/doi/abs/10.1029/2005JB003861> doi: 10.1029/2005JB003861
- Wauthier, C., Roman, D. C., & Poland, M. P. (2019, June). Modulation of seismic activity in Kilauea's upper East Rift Zone (Hawaii) by summit pressurization. *Geology*, 47(9), 820–824. Retrieved 2021-09-01, from <https://doi.org/10.1130/G46000.1> doi: 10.1130/G46000.1
- Wech, A. G., Thelen, W. A., & Thomas, A. M. (2020, May). Deep long-period earthquakes generated by second boiling beneath Mauna Kea volcano. *Science*, 368(6492), 775–779. Retrieved 2022-06-02, from <https://www.science.org/doi/10.1126/science.aba4798> doi: 10.1126/science.aba4798
- Wilding, J. D., Zhu, W., Ross, Z. E., & Jackson, J. M. (2023, February). The magmatic web beneath Hawai'i. *Science*, 379(6631), 462–468. Retrieved 2023-06-29, from <https://www.science.org/doi/10.1126/science.ade5755> (Publisher: American Association for the Advancement of Science) doi: 10.1126/science.ade5755
- Wolfe (compiler), E. W., & Morris, J. (1996). *Geologic map of the Island of Hawaii* (Tech. Rep. No. 2524-A). U.S. Geological Survey. Retrieved 2022-11-03, from <https://pubs.er.usgs.gov/publication/i2524A> (ISBN: 9780607860825 Publication Title: IMAP) doi: 10.3133/i2524A
- Woods, J., Winder, T., White, R. S., & Brandsdóttir, B. (2019, January). Evolution of a lateral dike intrusion revealed by relatively-relocated dike-induced earthquakes: The 2014–15 Bárarbunga–Holuhraun rifting event, Iceland. *Earth and Planetary Science Letters*, 506, 53–63. Retrieved 2024-01-23, from <https://www.sciencedirect.com/science/article/pii/S0012821X18306289> doi: 10.1016/j.epsl.2018.10.032

- Wright, T. L., & Klein, F. W. (2006, March). Deep magma transport at Kilauea volcano, Hawaii. *Lithos*, 87(1), 50–79. Retrieved 2022-03-28, from <https://www.sciencedirect.com/science/article/pii/S0024493705001350> doi: 10.1016/j.lithos.2005.05.004
- Wyss, M., Liang, B., Tanigawa, W. R., & Wu, X. (1992). Comparison of orientations of stress and strain tensors based on fault plane solutions in Kaoiki, Hawaii. *Journal of Geophysical Research: Solid Earth*, 97(B4), 4769–4790. Retrieved 2024-01-23, from <https://onlinelibrary.wiley.com/doi/abs/10.1029/91JB02968> doi: 10.1029/91JB02968
- Zaliapin, I., & Ben-Zion, Y. (2013). Earthquake clusters in southern California I: Identification and stability. *Journal of Geophysical Research: Solid Earth*, 118(6), 2847–2864. Retrieved 2021-01-19, from <https://agupubs.onlinelibrary.wiley.com/doi/abs/10.1002/jgrb.50179> doi: <https://doi.org/10.1002/jgrb.50179>
- Zhu, W., & Beroza, G. C. (2019, January). PhaseNet: a deep-neural-network-based seismic arrival-time picking method. *Geophysical Journal International*, 216(1), 261–273. Retrieved 2023-07-07, from <https://doi.org/10.1093/gji/ggy423> doi: 10.1093/gji/ggy423
- Zhu, W., McBrearty, I. W., Mousavi, S. M., Ellsworth, W. L., & Beroza, G. C. (2022). Earthquake Phase Association Using a Bayesian Gaussian Mixture Model. *Journal of Geophysical Research: Solid Earth*, 127(5), e2021JB023249. Retrieved 2024-01-23, from <https://onlinelibrary.wiley.com/doi/abs/10.1029/2021JB023249> doi: 10.1029/2021JB023249